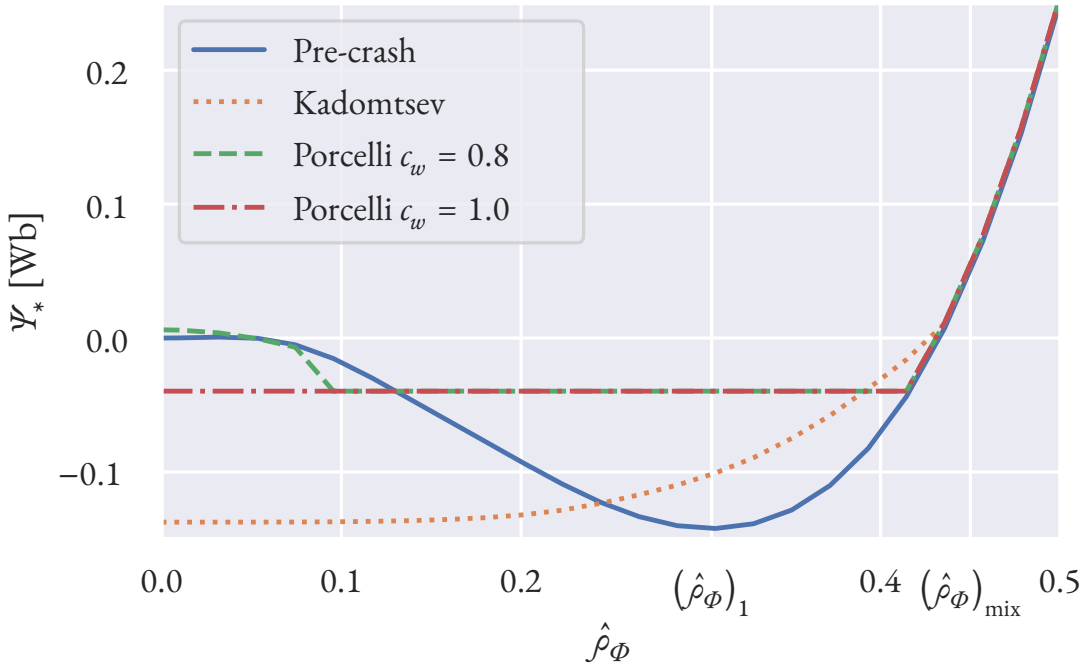

Simulating the Sawtooth Instability in Tokamak Plasmas

Implementation in the European Transport Simulator (ETS)

Master's thesis in Physics and Astronomy

ISAK LARSÉN

DEPARTMENT OF SPACE, EARTH AND ENVIRONMENT

CHALMERS UNIVERSITY OF TECHNOLOGY
Gothenburg, Sweden 2025
www.chalmers.se

Master's thesis 2025

Simulating the Sawtooth Instability in Tokamak Plasmas

Implementation in the European Transport Simulator (ETS)

ISAK LARSÉN

CHALMERS
UNIVERSITY OF TECHNOLOGY

Department of Space, Earth and Environment
Division of Astronomy and Plasma Physics
Plasma Physics and Fusion Energy
Chalmers University of Technology
Gothenburg, Sweden 2025

Simulating the Sawtooth Instability in Tokamak Plasmas
Implementation in the European Transport Simulator (ETS)
ISAK LARSÉN

Supervisor: Dmitro Yadykin, Department of Space, Earth and Environment
Examiner: Pär Strand, Department of Space, Earth and Environment

Master's Thesis 2025
Department of Space, Earth and Environment
Division of Astronomy and Plasma Physics
Plasma Physics and Fusion Energy
Chalmers University of Technology
SE-412 96 Gothenburg
Sweden
Telephone +46 31 772 1000

Cover: Pre-crash and crash helical flux Ψ_* profiles, for an event of a sawtooth crash in JET shot 99971 according to the Kadomtsev and Porcelli (with $c_w = 0.8$ and 1.0) models. Shown with respect to the normalised generalised toroidal flux coordinate $\hat{\rho}_\Phi$.

Typeset in LaTeX
Printed by Chalmers Digital Printing
Gothenburg, Sweden 2025

Simulating the Sawtooth Instability in Tokamak Plasmas
Implementation in the European Transport Simulator (ETS)
ISAK LARSÉN
Department of Space, Earth and Environment
Chalmers University of Technology

Abstract

The sawtooth instability is an internal kink instability or a resistive $m = 1$ instability in tokamak plasmas, that cause sudden, near instantaneous, disruptions regularly, which results in a characteristic sawteeth wave in the power output of a tokamak fusion reactor. When ITER, the largest tokamak reactor in the world, will be taken into operation it is important that all known physics is included in the simulations, that will guide the operation for optimal efficiency. The European Transport Simulator (ETS) is a large integrated workflow for simulating tokamak plasmas, that could provide ITER with the necessary simulation data. This thesis uses an existing implementation of the Kadomtsev and Porcelli models for the simulations of the sawtooth instability, after updating the code to be compatible with newer versions of the Integrated Modelling & Analysis Suite (IMAS) infrastructure in the Persistent Actor Framework (PAF), which the latest version of ETS is built on, to simulate a sawtooth crash in a JET plasma. The theoretical reasoning for these two models is explained in order to later make it clear that the results from the simulations are what is expected from an accurate implementation of the models. The presented results are from a test workflow, that only include the actors created from the updated sawtooth model implementation and saves their final output. Unfortunately, it will be clear that neither of the two models, in present representation, will provide post-crash profiles that are well enough behaved to be used in any time progressive simulation in a meaningful way, but it is argued that this issue can be solved in future work, perhaps through implementing a flat-current model (FCM), or updating the implementation of the existing models.

Keywords: plasma physics, fusion, magneto hydro dynamics (MHD), tokamak, sawtooth instability, the International Thermonuclear Experimental Reactor (ITER), the Joint European Torus (JET), European Transport Simulator (ETS).

Acknowledgements

First and foremost, I want to thank my supervisor Dmitro Yadykin, for giving me the opportunity to do this project in the exciting field of plasma physics and fusion energy, as well as Francesca Poli at ITER, who has acted as a second supervisor in all ways that matter. You have both been very generous with your time and provided all the help and guidance I needed throughout this project.

Also, I want to give many thanks to my examiner Pär Strand, for making sure to be aware of my progress throughout the entire process. This is an example of the great leadership you, from what I have seen, provide for everyone working in the Plasma Physics and Fusion Energy group. A group consisting of all around good people, bond together by a very strong team spirit, who all have made me feel very included.

A special thanks to Charbel Nemer, another master student, who has worked on a parallel thesis project on the related (but different) neoclassical tearing mode (NTM) instability. Our discussions about the most difficult aspects of the field of plasma physics in general and our chosen subjects of focus in particular, has greatly increased the level of understanding I have been able to reach.

I want to thank my parents and my brother for all the love and support for all aspects of life. I am especially thankful for you being there for me through all of the many years of studying at Chalmers. Some of those years were particularly difficult and my ability to reach this point of triumph is greatly thanks to the firm ground to stand on that you have given me.

Finally, thank you Amanda, my partner. Having you by my side has made a major improvement in my life and you have certainly given me the strength to finish this thesis in an at least somewhat decent matter. I hope that you feel as much of my love for you as I feel yours.

Isak Larsén, Gothenburg, November 2025

Acronyms

CPO consistent physical object. 16, 29

ETS European Transport Simulator. v, 1, 2, 15, 16, 27, 29

FCM flat-current model. v, 9, 13, 27, 29

IDS interface data structure. 15, 16, 17, 28, 29

IMAS Integrated Modelling & Analysis Suite. v, 1, 15, 16, 29

ITER the International Thermonuclear Experimental Reactor. v, vii, 1, 7, 15, 30

JET the Joint European Torus. v, 16, 19, 21, 23, 24

KO Kruskal–Oberman. 10

MHD magneto hydro dynamics. v, 5, 6, 7, 10

MUSCLE 3 Multiscale Coupling Library and Environment version 3. 15

NTM neoclassical tearing mode. 2, 13, 30

PAF the Persistent Actor Framework. v, 1, 2, 15, 16, 29

yMMSL the YAML version of the Multiscale Modelling and Simulation Language. 15

Nomenclature

Below is the nomenclature of physical constants, coordinates, fields & profiles, variables, and parameters that have been used throughout this thesis.

Physical constants

μ_0	Vacuum permeability

Coordinates

(x, y, z)	Cartesian coordinates
(r, θ, ϕ)	Toroidal coordinates (minor radius, poloidal angle, toroidal angle)
R	Major radius coordinate
$\hat{\boldsymbol{R}}$	Unit vector in the major radial direction
t	Time
$\hat{\rho}_\Phi$	Normalised toroidal flux coordinate

Fields & profiles

$\boldsymbol{B}$	Magnetic field
B	Magnetic field strength
B_ϕ	Toroidal magnetic field strength
B_θ	Poloidal magnetic field strength
B_*	Helical magnetic field strength
$\boldsymbol{E}$	Electric field
$\boldsymbol{j}$	Current density
j_ϕ	Toroidal current density
K	Helicity
n_e	Electron density
p	Pressure
q	Safety factor

q_e	Electric charge
T_e	Electron temperature
$\boldsymbol{v}$	Centre of mass fluid velocity
$\boldsymbol{v}_{\nabla B}$	∇B drift velocity
$\boldsymbol{v}_{\boldsymbol{E}\times\boldsymbol{B}}$	$\boldsymbol{E} \times \boldsymbol{B}$ drift velocity
ρ_m	Mass density
Ψ_*	Helical magnetic flux
$\hat{\Psi}_*$	Normalised helical magnetic flux

Variables

m, n	Poloidal mode number, toroidal mode number
r_{K}	Final radius of a reconnected helical flux surface in the Kadomtsev model
r_{Li}	Thermal ion Larmor radius
r_{mix}	Mixing radius
$\bar{r}_1$	Average radius of a $q = 1$ surface
r_+	Radius of outer equal helical flux surface
r_-	Radius of inner equal helical flux surface
s_1	Magnetic shear at a $q = 1$ surface
δW	Variation in energy
γ	The ratio of specific heats
γ_{L}	Characteristic growth rate of the internal king mode in the ion-kinetic regime
η	Electrical resistivity
τ_{A}	Alfvén time
ω_{Dh}	Fast trapped ion precessional drift frequency
$\omega_{*\mathrm{i}}$	Diamagnetic frequency

Parameters

a	The minor radial size of a tokamak
$B_{\phi 0}$	Vacuum toroidal magnetic field strength at $R = R_0$
$c_{\mathrm{h}}, c_{\mathrm{mod}}, c_{\mathrm{L}}, c_*$	Numerical factors that control the importance of each crash condition
c_w	Numerical factor to regulate the critical island width
R_0	The major radial size of a tokamak
w_{crit}	Critical island width
ϵ	The inverse aspect ratio of a tokamak

Contents

List of Figures

1

Introduction

To combat the global warming, caused by the green house emissions from our modern society, a green transition in power generation is necessary. For many countries, a large part of this will mostly be achieved through nuclear energy. It is commonly known that nuclear power generation through fission results in dangerous and weaponisable nuclear waste, which is not the case for nuclear fusion.

Fusion has for some time been considered as a possible source of power for our modern society, but the performance of the commonly considered scheme for fusion reactors, i.e. tokamak, is limited (among other mechanisms) by instabilities accrued in the plasma. For tokamak reactors to work properly, it is therefore needed to carefully model and regulate said instabilities. One of these is the sawtooth instability, which is a characteristic performance limiting instability.

To study the stability of fusion plasmas and its effects on the performance for the realistic scenarios, complex numerical simulations needs to be performed using integrated workflows that combine the models for different physical phenomena. The European Transport Simulator (ETS) is one of these workflows and in its latest version, which is currently being developed, integration is done through the Integrated Modelling & Analysis Suite (IMAS) infrastructure. In this new infrastructure the modules are implemented as actors according to the Persistent Actor Framework (PAF), which allows for easier integration between all modules written in different languages by many people in different teams. A sawtooth model was included in the previous version of ETS, but at the start of this thesis project, it was incompatible with the new infrastructure and framework.

The International Thermonuclear Experimental Reactor (ITER) is the largest fusion reactor in the world and is currently being built in France. It will be used to further improve the experimental understanding of tokamak fusion reactors when put into operation and in preparation of this, it is important to have as good relevant simulation data as possible. This is because the reactor needs to be regulated to keep it within foreseen operating conditions. The sawtooth instability is certainly important to include in these simulations, since it regularly causes major disruptions that limit power output and can trigger other instabilities that also are detrimental for efficiency or confinement. The work behind this thesis has therefore been done in close collaboration with ITER team, to make sure it is as relevant for them as possible.

1.1 Thesis aim, specification, and limitations

The performance of the tokamak plasma is limited by the sawtooth instability, which therefore needs to be included in simulations for accurate predictions of the evolution of kinetic profiles

(density, temperature). Therefore, this project is aimed to update the previously implemented model for sawtooth instability, to comply with all the requirements posed by a PAF version of ETS. Additionally, tests were to be conducted, to ensure that the implementation of the model still works properly and that the update was done correctly.

At the beginning of this project, the following questions where specified to be answered at its completion:

- Do the actors correctly capture the physical processes involved in the sawtooth crash and reconnection?
- Are the kinetic profiles evolving as expected with the evolution of sawteeth, as compared to the referenced results found in (Fischer et al. 2019; Igochine 2023)?
- Are the sawtooth actors correctly coupled to the neoclassical tearing mode (NTM) actors in a test workflow?

These questions turned out to be more ambitious than anticipated and the reader will find that only the first of these three questions can be given the satisfying answer "yes".

The scope of this thesis was initially limited by studies of the sawtooth instability and its direct synergy with other physics models, e.g. the NTM model, which has been worked on by another master student simultaneously. But unfortunately, due to the limited time available and the complexity of the project being more difficult than expected, the scope needed to be further limited to focus on the sawtooth crash event and the physics behind the reconnection process, which is why only the first of the three specified questions can receive a satisfying answer.

Hopefully, the narrowing of the scope is made up for by the explanations of the physics of the sawtooth instability from a theoretical perspective in chapter 2 and the simulation framework and implementation are described in chapter 3. The results from the simulations are shown in chapter 4, which are compared in detail in chapter 5 with what should be expected from the theory. Towards the end of the thesis, it will also be made clear what obstacles has made it difficult to include the sawtooth actors in the type of simulations that involves time evolution, which is required to be able to be fully satisfied with the answers to the remaining questions above.

1.2 What is plasma? And why it matters for fusion energy

Plasma is a state of matter, often considered the fourth after solid, liquid, and gas, where the temperature is so high that a significant proportion of the molecules and atoms will become ionised. Throughout the universe plasma is actually the most common state of matter, for instance in the stars, solar wind, interstellar medium, in aurora borealis in the atmosphere of Earth or other planets, or in human made fusion reactors. The conditions are of course very different between these places causing different phenomena, so they can be thought of as different types of plasma.

Fusion occurs naturally at a significant rate in stars, due to the high gravitational pressure pulling the plasma together, but for plasma reactors on Earth this way of confinement is not an option in general[1], for the obvious reason of the lack of enough mass. In addition, simply keeping

[1] Although, inertial confinement fusion tries to mimic this with lasers.

plasma in a “normal” vessel, i.e. anything similar to how we contain chemicals, pressurised gases, liquid nitrogen, etc., is not a good idea, since the really hot temperatures would destroy any solid material in direct contact. In stead, the most common method for fusion reactor plasma confinement is to have strong magnetic fields configured such that the electromagnetic forces keeps most of the electrons and ions away from the inner walls.

2

Theory

Due to the significant proportion of charged particles, plasmas are very much affected by electro dynamics, in addition to the collisions of "normal" fluid dynamics. A model where all particles are considered as a single fluid under the influence of Maxwell's equations will therefore be covered, after which there will be a brief explanation of how plasma instabilities can be explained through the energy principle. Thereafter, the tokamak concept of plasma confinement in fusion reactor will be explained, in enough detail that all relevant concepts for the sawtooth instability should be clear.

Of course, the sawtooth instability, that is the focus of this thesis, will be thoroughly explained from a theoretical standpoint. The Kadomtsev and Porcelli models of the sawtooth instability will be covered in detail and a flat-current model (FCM) will be mentioned as a potential candidate to avoid some of their issues.

2.1 Magneto hydro dynamics (MHD)

Plasma can often be modelled as a single fluid in magneto hydro dynamics (MHD), that is a combination of fluid dynamics and electro magnetics. The equations are therefore a combination of the conservation laws in fluid dynamics and Maxwell's equations in electro magnetics and read

$$\frac{\partial \rho_m}{\partial t} + \boldsymbol{\nabla} \cdot \left(\rho_m \boldsymbol{v}\right) = 0, \quad \text{(mass continuity equation)}, \tag{2.1}$$

$$\frac{\mathrm{d}}{\mathrm{d}t}\left(\frac{p}{\rho_m^{\gamma}}\right) = 0, \quad \text{(adiabatic equation of state)}, \tag{2.2}$$

$$\rho_m \frac{\mathrm{d}\boldsymbol{v}}{\mathrm{d}t} = \boldsymbol{j} \times \boldsymbol{B} - \boldsymbol{\nabla} p, \quad \text{(momentum equation)}, \tag{2.3}$$

$$\boldsymbol{\nabla} \times \boldsymbol{B} = \mu_0 \boldsymbol{j}, \quad \text{(Ampère's law)}, \tag{2.4}$$

$$\boldsymbol{\nabla} \times \boldsymbol{E} = -\frac{\partial \boldsymbol{B}}{\partial t}, \quad \text{(Faraday's law)}, \tag{2.5}$$

$$\boldsymbol{\nabla} \cdot \boldsymbol{B} = 0, \tag{2.6}$$

$$\boldsymbol{E} + \boldsymbol{v} \times \boldsymbol{B} = \eta \boldsymbol{j}, \quad \text{(resistive Ohm's law)}, \tag{2.7}$$

where ρ_m is the mass density, t is time, $\boldsymbol{v}$ is the fluid velocity,

$$\frac{\mathrm{d}}{\mathrm{d}t} \equiv \frac{\partial}{\partial t} + \boldsymbol{v} \cdot \boldsymbol{\nabla}$$

is the convective derivative, p is the pressure, γ is the ratio of the specific heats, $\boldsymbol{j}$ is the current density, $\boldsymbol{B}$ is the magnetic field, μ_0 is the vacuum permeability, $\boldsymbol{E}$ is the electric field, and η is the electrical resistivity. Additionally, many plasma phenomena are adequately described when using the ideal Ohm's law in stead of the resistive one in equation (2.7), that is letting $\eta = 0$. To differentiate between what of the two versions of Ohm's law is used one can specify ideal or resistive MHD.

2.2 Energy principle and equilibrium stability

Similarly to other fields of physics, the energy principle can be used to determine the stability of an MHD calculated equilibrium in a plasma. That is, considering the variation in potential energy δW from a small perturbation from the equilibrium state and use the fact that any physical system will tend to minimising its energy according to the energy principle. In other words, the equilibrium is *stable* if $\delta W > 0$, since it means the energy is locally minimised, which results in the plasma to fall back to its equilibrium state after any small perturbation, but the equilibrium is *unstable* if $\delta W < 0$, since the energy is locally maximised in that case, making the plasma diverge into a new equilibrium at a lower energy after similar perturbations (Bellan 2006). Tokamak MHD instabilities can be divided in the following categories (Wesson 2004):

(i) *Kink instability*, an ideal MHD instability, that leads to kinking of the magnetic surfaces and the plasma boundary, without affecting the topology. It is driven by the current gradient or pressure gradient.

(ii) *Tearing mode*, a resistive MHD, causing tearing and rejoining of magnetic field lines, affecting the topology. It is driven by the current gradient.

(iii) *Internal kink*, an ideal MHD instability with poloidal mode number $m = 1$ and toroidal mode number $n = 1$, with its resonant surface being given by $q = 1$, requiring such a surface to exist in the plasma for this instability to occur. It mostly affects the plasma core where $q \lesssim 1$, but the topology remains unchanged.

(iv) *Resistive $m = 1$ instability*, similar to the internal kink, but with a resistive layer around the resonant ($q = 1$) surface that can result in kinking or tearing, modifying the topology.

(v) *Ballooning modes*, a local instability driven by the pressure gradient.

(vi) *Mercier instability*, a limiting ballooning mode.

(vii) *Vertical instability*, an instability driven by plasma elongation.

Most of these are outside the scope of this thesis, but the sawtooth instability, which is the focus of this thesis, is a resistive $m = n = 1$ kink instability (Chapman 2015; Wesson 2004).

2.3 The tokamak scheme and toroidal geometry

One way to contain and stabilise plasma for fusion power generation purposes is the Tokamak scheme, where the plasma is kept in a toroidal (doughnut) shape by a helically shaped magnetic field, confining the charged particles in approximately circular orbits around the major axis of the torus. The word tokamak is in fact a Russian acronym[1] that stands for toroidal chamber

[1] Токамак, тороидальная камера с магнитными катушками, toroidal'naya kamera s magnitnymi katushkami

with magnetic coils. The toroidal geometry, see figure 2.1, means it is convenient to use a toroidal coordinate system (r, θ, ϕ), that is the minor radius r, the poloidal angle θ, and the toroidal angle ϕ They are defined such that the standard Cartesian coordinates (x, y, z) can be expressed

$$\begin{cases} x = (R_0 + r\sin\theta)\cos\phi, \\ y = (R_0 + r\sin\theta)\sin\phi, \\ z = r\cos\theta, \end{cases}$$

where R_0 is the distance of the centre of the core to the central poloidal axis, i.e. the z axis, of the tokamak, or in other words its major radial R coordinate.

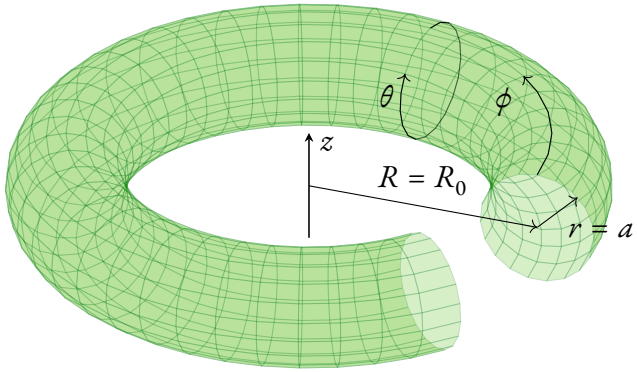

Figure 2.1: Schematic of the plasma core in a tokamak. Marked poloidal axis z, major radius R, minor radius r, poloidal angle θ, and toroidal angle ϕ. The centre of the core is at major radius $R = R_0$ and minor radius $r = 0$, while the edge of the core is at major radius $R = R_0$ and minor radius $r = a$.

The MHD equations are quite complicated and computationally expensive to solve in 3D, so many models of tokamak phenomena adopt the simplified cylindrical approximation. That is, if the major radius of a tokamak is significantly larger than its minor radius, a short element of the torus can be approximated as a cylinder, so any physical quantity can be expressed in terms of a single radial coordinate due to symmetry. In other words only the leading order term is considered when Taylor expanding with respect to the inverse aspect ratio

$$\varepsilon = \frac{a}{R_0},$$

where a is the size of the core in the minor radial direction r, see figure 2.1. Despite many actual tokamaks being far from fulfilling $\varepsilon \ll 1$, e.g. $\varepsilon \approx 0.3$ for ITER, it holds in the centre of the plasma where r is significantly smaller than a meaning the effective $\varepsilon_{\text{eff.}} \ll 1$. This approximation is essential for many physical models for tokamak plasmas and the sawteeth models used in this thesis does indeed use them.

Due to the toroidal geometry, see figure 2.1, the magnetic field strength varies along the major radius R of the tokamak

$$B \equiv |\boldsymbol{B}| = B_{\phi 0}\frac{R_0}{R} + \mathcal{O}(\varepsilon),$$

where $B_{\phi 0}$ is the vacuum toroidal magnetic field strength at $R = R_0$. This results in

$$\nabla B = -B_{\phi 0}\frac{R_0}{R^2}\hat{\boldsymbol{R}} + \mathcal{O}(\varepsilon),$$

which causes a ∇B drift for particles of charge q_e

$$\boldsymbol{v}_{\nabla B} \propto \frac{1}{q_e}\boldsymbol{B} \times \nabla B,$$

that is one of several drift effects that generally occur in plasmas, perpendicular to the magnetic field and the radially directed gradient. Importantly, this drift is in opposite directions for positively and negatively charged particles, due to the q_e dependence, so it will result in a charge disparity in the plasma, giving rise to an electric field $\boldsymbol{E}$ (parallel with $\boldsymbol{v}_{\nabla B}$ and therefore perpendicular to $\boldsymbol{B}$), which results in a $\boldsymbol{E} \times \boldsymbol{B}$ drift

$$\boldsymbol{v}_{\boldsymbol{E}\times\boldsymbol{B}} \propto \boldsymbol{E} \times \boldsymbol{B},$$

which is another generally occurring plasma drift, but this is not charge dependent.

Because of these drifts, a straight toroidal, i.e. ϕ directional, magnetic field

$$B_\phi = B_{\phi 0}\frac{R_0}{R}\left(1 + \mathcal{O}\left(\varepsilon^2\right)\right)$$

is not enough to create a stable plasma, since all electrons and ions would drift to and collide with the top or bottom part of the inner wall of the tokamak. The magnetic field must therefore contain a poloidal twist

$$B_\theta \sim \varepsilon B_{\phi 0},$$

which is achieved through a toroidal plasma current density j_ϕ.

2.4 The safety factor q, helical magnetic field B_*, and helical flux Ψ_*

How much the magnetic field is twisted can be measured with the safety factor

$$q \equiv \frac{\Delta\phi}{2\pi} = \frac{rB_\phi}{R_0 B_\theta} + \mathcal{O}(\varepsilon), \tag{2.8}$$

where $\Delta\phi$ represents how far toroidally it takes the magnetic field to make a complete poloidal twist, i.e. $\Delta\theta = 2\pi$. It is called the safety factor because higher q typically results in higher plasma stability, e.g. if $q > 1$ everywhere in the plasma the sawtooth instability will not occur (Wesson 2004).

Now, consider a helical sheet defined ${}^{\mathrm{d}\theta}/_{\mathrm{d}\phi} = 1$ and realise that the magnetic field lines will lie in such a sheet for a $q = 1$ surface, while it will be intersected by the field lines where $q \neq 1$. We can therefore define the helical magnetic field, i.e. the component of the total magnetic field that crosses the helical sheet (ibid.),

$$B_* \equiv \frac{1}{\sqrt{1 + {}^{r^2}/_{R^2}}}\left(B_\theta - \frac{r}{R}B_\phi\right) = B_\theta\left(1 - q\right) + \mathcal{O}(\varepsilon), \tag{2.9}$$

which is perpendicular to the helical sheets and in turn the helical flux Ψ_*, such that

$$\frac{\mathrm{d}\Psi_*}{\mathrm{d}r} \equiv B_*, \tag{2.10}$$

so the normalised helical flux

$$\hat{\Psi}_*(r^2) \equiv \frac{R}{2B_\phi}\Psi_*(r^2) = \int_0^{r^2} \left(q^{-1} - 1\right) \mathrm{d}r'^2, \tag{2.11}$$

in the cylindrical approximation (Porcelli et al. 1996). Note that, Ψ_* is locally extreme at a $q = 1$ surface, since

$$\frac{\mathrm{d}\Psi_*}{\mathrm{d}r} = B_* = 0$$

and constant flux surfaces on one side of said surface will therefore have corresponding surfaces on the other side at equal constant flux.

2.5 What is the sawtooth instability?

The sawtooth instability is named due to the characteristic sawtooth wave in average core temperature, core density, and therefore in the power output of the entire reactor, it causes, see figure 2.2. The sawtooth period can be divided into three phases (Chapman 2015): (i) the ramp phase, when density and temperature increase gradually, leading to a similar increase in power, (ii) the precursor phase, when a helical magnetic perturbation gradually grows until (iii) the fast collapse or sawtooth crash, when the core temperature and core density drop so rapidly it is almost instant compared to other relevant processes. Additionally, during the sawtooth ramp, the radial profile of q also changes at a slow rate, eventually making a $q = 1$ surface with growing radius r_1 during the precursor phase, until the sawtooth crash is triggered by the onset of an internal kink mode with toroidal $n = 1$ and poloidal $m = 1$ mode numbers ($m = 1$ mode), at which, through a process of reconnection of surfaces of equal helical flux Ψ_* on either side of the $q = 1$ surface, the q profile snaps back to be more flat in the plasma core and therefore remove or blur the distinct $q = 1$ surface. At the same time the transport of energy is enhanced, meaning that the energy is expelled from the central region towards the edge.

A basic model for sawtooth instability was developed by Kadomtsev in the seventies (Wesson 2004). The model qualitatively describes the mechanism of sawtooth crash, but inconsistencies are found between the Kadomtsev model and experimental results, especially in large tokamaks. Therefore, other, more complex, models have been developed over the years since. The Porcelli model, developed in the 90's, is only slightly more complex, including explicit conditions for the sawtooth crash and allowing for incomplete reconnections (Porcelli et al. 1996). The flat-current model (FCM) is an even more complicated model and was developed another two decades later, which could provide more physical accuracy by eliminating the unphysical current sheets, that are unfortunate features of the older models (Fischer et al. 2019). This last model is however not covered in this thesis, due to time restraints, but it is mentioned here because of it potentially being of interest in future work.

The q profile pre-crash is almost the same in the Kadomtsev and Porcelli models, that is $q < 1$ in the centre and smoothly increases such that $q > 1$ beyond r_1. In contrast, the crash q profile is clearly different between the two models, since the Kadomtsev stays mostly smooth, starting at $q = 1$ in the centre and slowly increasing radially until there is a sudden jump, causing a current sheet, whereas it is piecewise flat for the Porcelli model, being $q < 1$ in the centre, $q = 1$ in a region around r_1, and a similar current sheet as in the Kadomtsev model. These two models will be explained in detail later in this chapter and are also sometimes called complete (Kadomtsev) and incomplete (Porcelli) reconnection, which is related to this difference.

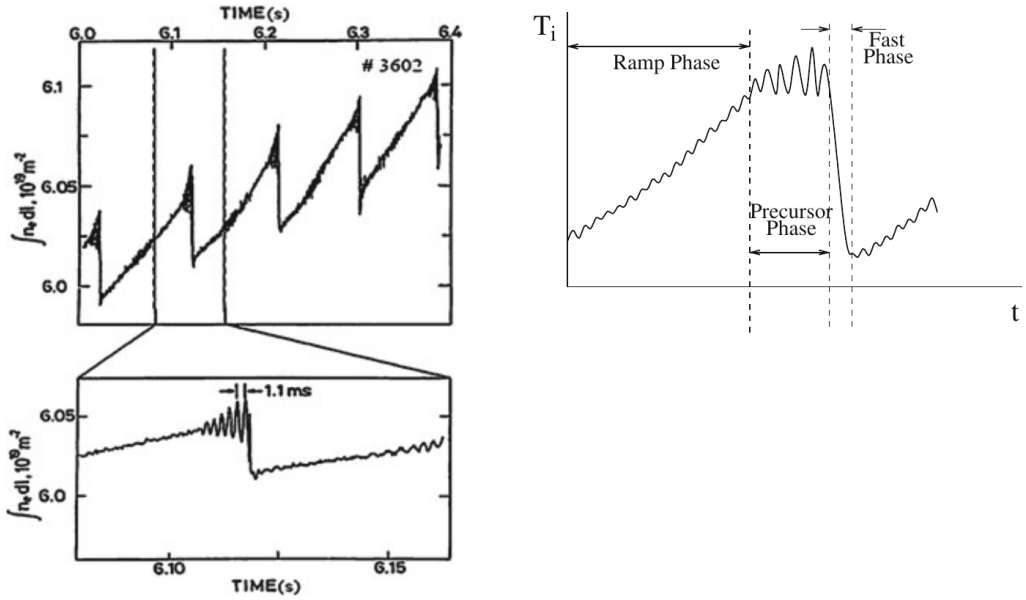

Figure 2.2: The three phases of sawteeth, being the ramp phase, the precursor phase, and the fast phase, seen in the line-integrated electron density of a JET plasma. Credit: Ian T. Chapman (2015). "Sawtooth Instability". In: *Active Control of Magneto-hydrodynamic Instabilities in Hot Plasmas*. Ed. by Valentin Igochine. Springer Series on Atomic, Optical, and Plasma Physics (SSAOPP), vol. 83. Springer Berlin Heidelberg. Chap. 4, pp. 105–142. ISBN: 978-3-662-44222-7. DOI: 10.1007/978-3-662-44222-7_4.

2.5.1 Conditions for crash

In the same paper as where the incomplete reconnection model was introduced, Porcelli et al. showed that the conditions for the sawtooth crash to occur can be determined from the variation in the potential energy of the mode

$$\delta W = \delta W_{\text{core}} + \delta W_{\text{fast}},$$

where δW_{fast} is the term for fast particles and δW_{core} is the core plasma potential energy, that is defined

$$\delta W_{\text{core}} = \delta W_{\text{MHD}} + \delta W_{\text{KO}},$$

where δW_{MHD} is the ideal MHD term and δW_{KO} is the Kruskal–Oberman (KO) term, which describes collisionless thermal ions (Chapman 2015). The crash is triggered when one of the following conditions are met:

$$-\delta W_{\text{core}} > c_{\text{h}} \omega_{\text{Dh}} \tau_{\text{A}}, \tag{2.12}$$

$$-\delta W > \frac{1}{2} c_{\text{mod}} \omega_{*\text{i}} \tau_{\text{A}}, \tag{2.13}$$

$$-c_{\text{L}} \hat{r}_{\text{L}} < -\delta W < \frac{1}{2} c_{\text{mod}} \omega_{*\text{i}} \tau_{\text{A}} \qquad \text{and} \qquad \omega_{*\text{i}} < c_{*} \gamma_{\text{L}}, \tag{2.14}$$

where τ_{A} is the Alfvén time, $\omega_{*\text{i}}$ is the diamagnetic frequency, γ_{L} is the characteristic growth rate of the internal kink mode in the ion-kinetic regime, $\hat{r}_{\text{L}} = r_{\text{Li}}/\bar{r}_1$, where r_{Li} is the thermal ion Larmor radius and $\bar{r}_1$ is the average radius of the $q = 1$ surface, and ω_{Dh} is the fast trapped

ion (high energy) precessional drift frequency, while c_{h}, c_{mod}, c_{L}, and c_* are numerical factors of order unity that control the importance of different contributions.

The condition in equation (2.12) describes when ω_{Dh} is too low for the fast ions to have a stabilising effect via the third adiabatic invariant, that is the magnetic flux. The condition in equation (2.13) cover when layer physics cease to be stabilising, which is something I personally do not understand at the moment. The condition in equation (2.14) also includes a condition for when $\omega_{*\mathrm{i}}$ is too low for the diamagnetic and electron drift effects in combination with the plasma viscosity to be stabilising with respect to the $m = 1$ mode.

2.5.2 Changes to the profiles during crash

At crash event there is a near-instant transport of fast electrons and ions from hotter to cooler regions of the plasma. This results in a flattening of the electron and ion temperatures and densities, which is also observed in experiments where sawtooth oscillations are present. Typically this flattening only occurs within a certain *inversion* or *mixing radius* r_{mix}, outside of which the temperature and density remain the same.

2.5.2.1 Complete reconnection (the Kadomtsev model)

The complete reconnection (Kadomtsev 1975) model is, in addition to equal helical flux surfaces reconnecting, based on the assumption that the toroidal flux is conserved, which implies that the cross sectional area between the reconnecting surfaces will be conserved. The rapid crash process will in that case consist of a growing $m = 1$ island, where each constant Ψ_* surface, at some radius r_- within the $q = 1$ surface at r_1, moves until it touches the corresponding equal helical flux surface at radius $r_+ > r_1$, shown in figure 2.3. The area between the two equal helical flux surfaces is clearly

$$A = \pi\left(r_+^2 - r_-^2\right)$$

in the initial step in figure 2.3a, so the final radius r_{K} of the reconnected helical flux surface is given by

$$r_{\mathrm{K}}^2 = r_+^2 - r_-^2, \tag{2.15}$$

since the area conservation leads the same $A = \pi r_{\mathrm{K}}^2$ in the final step in figure 2.3c. The (final) relaxed helical flux Ψ_*^{f} can now be expressed in terms of the (initial) pre-crash helical flux Ψ_*^{i}

$$\Psi_*^{\mathrm{f}}(r_{\mathrm{K}}) = \Psi_*^{\mathrm{i}}(r_-) = \Psi_*^{\mathrm{i}}(r_+), \tag{2.16}$$

for $0 \leq r_{\mathrm{K}} \leq r_{\mathrm{mix}}$, where r_{mix} is equal to the r_+ corresponding to $r_- = 0$.

2.5.2.2 Incomplete reconnection (the Porcelli model)

In the incomplete reconnection (Porcelli et al. 1996) model starts the reconnection process similarly to how it does in the Kadomtsev model, until the $m = 1$ island reaches some critical island width

$$w_{\mathrm{crit}} = 2\Big((r_{\mathrm{crit}})_+ - (r_{\mathrm{crit}})_-\Big),$$

see figure 2.4, or a dimensionless parameter c_w on the scale $0 \leq c_w \leq 1$, such that

$$w_{\mathrm{crit}} = 2c_w(r_{\mathrm{mix}})_{\mathrm{max}},$$

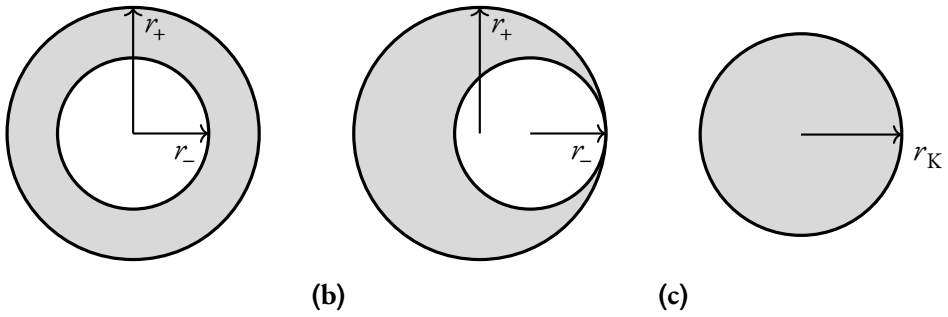

Figure 2.3: Equal helical flux surfaces during a complete reconnection process. (a) Equal helical flux surfaces before reconnection. (b) The helical flux surface originally at r_- starts to reconnect with the one at r_+ and forms an island shown as the shaded area. (c) The completed reconnection, after the island has been fully deformed into a circle keeping its area constant, resulting in the new surface having radius r_K.

where $(r_{mix})_{max}$ is the maximal possible mixing radius, which is equal to the r_{mix} of the Kadomtsev model. At this point the inner core ($0 \le r \le (r_{crit})_-$) goes through a process called Taylor relaxation, meaning the helicity of the pre-crash helical flux surface at the inside of the critical island

$$K\Big((r_{crit})_-\Big) \sim \int_0^{(r_{crit})_-} \left(\frac{q}{r^3}\right)^{-1} \mathrm{d}r \tag{2.17}$$

is conserved. This implies a flat $q^f(r) = q_0^f < 1$ profile for $0 \le r \le (r_{crit})_-$, where

$$\frac{1}{q_0^f} = \frac{4}{(r_{crit})_-} \int_0^{(r_{crit})_-} \frac{r^3}{q}\,\mathrm{d}r, \tag{2.18}$$

which in turn results in a parabolic $\Psi_*^f(r)$ for $0 \le r \le (r_{crit})_-$. Meanwhile, the island region is assumed to relax such that all of it will have the same helical flux

$$\Psi_*^f(r) = \text{constant} = \Psi_*^i\Big((r_{crit})_-\Big) \quad \text{for } (r_{crit})_- < r \le r_{mix} = (r_{crit})_+, \tag{2.19}$$

implying that

$$q^f(r) = \text{constant} = 1$$

in the same region. Note that $r_{mix} = (r_{crit})_+$ is smaller than the r_{mix} in the Kadomtsev model (unless in the case of $c_w = 1$ when they are still equal).

2.5.3 Issues with current sheets

The toroidal current distribution j_ϕ can be expressed in terms of q, since assumed toroidal symmetry, i.e.

$$\frac{\partial B_r}{\partial \theta} = 0$$

and

$$B_\theta \sim q^{-1}, \tag{2.20}$$

leads to Ampère's law in equation (2.4) simplifies to

$$j_\phi = \frac{1}{\mu_0}\frac{1}{r}\frac{\partial}{\partial r}(rB_\theta) = \frac{1}{\mu_0}\left(\frac{B_\theta}{r} + \frac{\partial B_\theta}{\partial r}\right) \sim \frac{1}{rq} + \frac{\partial}{\partial r}(q^{-1}), \tag{2.21}$$

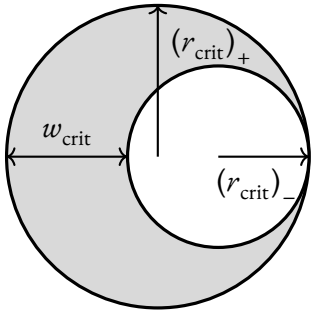

Figure 2.4: Equal helical flux surfaces during an incomplete reconnection process, shown when the critical island width w_{crit} have been reached, when the equal flux surfaces of radii $(r_{crit})_-$ and $(r_{crit})_+$ reconnect.

for the toroidal ϕ component of $\boldsymbol{j}$. Note that the $\partial/\partial r\left(q^{-1}\right)$ term means that any discontinuity in q will result in an infinite (or, in a numerical approximation, very large) j_ϕ spike at that point, which clearly is unphysical. When considering the entire geometry, these spikes represent strong current sheets, which are unfortunate features of both the Kadomtsev and Porcelli models. More advanced models exist, that combat this issue in various ways, the FCM (Fischer et al. 2019) being one example, which would result in over all more physically accurate results. However, this model is outside of the scope of this thesis due to the limited time available.

2.5.4 Triggering other instabilities

The new equilibrium that results from the crash event is not necessarily entirely stable either. In fact, the sawtooth crash can trigger other instabilities, such as an onset of a neoclassical tearing mode (NTM). In contrast to the sawtooth instability, which, as previously explained, causes a major transient event as soon as it is triggered, NTMs grow gradually over time, until they become large enough to cause significant disruptions. Therefore, despite being a trigger for NTMs in the first place, lowering the sawteeth period, i.e. making sawteeth crashes happen more often, has been proposed as a method of keeping NTM under control, since their growth will be reset at every sawtooth crash (Chapman 2015).

3

Simulation methods and implementation in the European Transport Simulator

ETS is an advanced modular simulator for tokamak plasmas. Throughout the years since its inception, it has been a product of constant development, in order to include more and more advanced and detailed physical models, that can provide more complete and accurate predictions for different scenarios. For all modules, each responsible for some particular physical aspect, to work as intended, despite being developed by many different people who might prefer different conventions etc., they need to follow some agreed upon framework that makes sure the data is sent between the modules in the same format, such that e.g. quantities are interpreted in the same units.

3.1 Interfacing in ETS workflow

The most resent version of ETS, currently being developed, uses the Multiscale Coupling Library and Environment version 3 (MUSCLE 3) framework to manage the large collection of programs that make up the complex simulator, written in different languages such as Python, C++, and Fortran (Veen et al. 2020). Exactly how the programs are connected, i.e. the workflow that needs to be run, is defined in yMMSL files[1], which may link to the programs directly or indirectly via other yMMSL files, i.e. sub-workflows. When considering a specific workflow yMMSL file, whether it links to physics model programs directly or sub-workflows, it is useful to think of them as singular entities, actors, that preform some sort of action on the data.

Additionally, this version of ETS uses the ITER developed IMAS infrastructure for standardisation of data formatting and follows PAF for integration of workflows. IMAS restricts the data transfer between the actors to the form of interface data structures (IDSs), whereas MUSCLE 3 by itself allows transfer of data in various other forms. PAF allows the actors to stay active during the entire workflow, which means they can remember the previous state (Coster 2024).

3.2 Updating previously implemented models

A combination of the Porcelli model and Kadomtsev model, Porcelli for the crash conditions and Kadomtsev for the changes in the profiles, as well as the full Porcelli model, were previously implemented for an older version of ETS (Merle 2015, 2016). This existing implementation was

[1]The acronym yMMSL stands for the YAML version of the Multiscale Modelling and Simulation Language.

in the form of three Fortran modules, one for the crash conditions, one for the calculation of the post-crash profiles, and one for updating the data structures with the new profiles, so a new equilibrium can be calculated in the next time step of ETS. Unfortunaly, the older version of ETS used a different framework that utilised consistent physical objects (CPOs) to send data between actors, which is incompatible with newer PAF versions of IMAS where IDSs are used in stead. In other words, the existing Fortran code needed to be changed such that it was compatible with the new framework and data structures, while allowing the overall structure and the implementation itself to stay intact.

The three upgraded sawteeth actors are connected in the following way in a PAF workflow (see figure 3.1): (i) the **sawcrit** actor receives input in the form of equilibrium, core profiles, and core transport IDSs, which it uses to calculate the crash conditions according to equations (2.12), (2.13), and (2.14), after which it sends all necessary data in a sawteeth IDS to (ii) the **sawcrash** actor, which, in the case of a sawtooth crash event, calculates most of the post-crash profiles and puts them in the sawteeth IDS, before sending it further to (iii) the **sawupdate** actor, which also receives the same versions of the equilibrium and core profile IDSs as sawcrit in order to update them with the post-crash profiles the sawcrash actor put in the sawteeth IDS, as well as the crash current density, which is calculated in sawupdate, which finally sends its output in the form of equilibrium, core profiles, sawteeth, and core instant changes IDSs. Note, that if the crash conditions are not met, sawcrash and sawupdate, simply just leaves the quantities unchanged in the output IDSs compared to the input IDSs.

3.3 Testing and validating

To verify the conversion from CPO to IDS was successful, the modified actors needed to be thoroughly tested. To do this, a test workflow was created where a basic initiation actor accesses a shot in the database and sends the correct IDSs as inputs to the sawteeth sub-workflow in figure 3.1, which output is sent to a basic finishing actor that saves the IDSs in a new run for that shot in the database. A the Joint European Torus (JET) shot numbered 99971 was chosen to use in this test, since there is a significant region where $q < 1$, so sawtooth crashes are expected and the post-crash profiles should show all the characteristics of the models with a clear $q = 1$ surface.

This test is only an interpretative one, i.e. the result is only valid for a single time step, but for the limited time available during this thesis project it is the best option. To simplify further, most of the crash conditions in equations (2.12), (2.13), and (2.14) were disabled and only a simplified version of the second condition in equation (2.13) remained. This condition is

$$s_1 > s_{\text{crit}},$$

where the magnetic shear s_1 at the $q = 1$ surface is larger than a set critical value s_{crit} and the magnetic shear s is defined

$$s = \frac{r}{q}\frac{\mathrm{d}q}{\mathrm{d}r}$$

(Antonsen et al. 1996). This simplification was done to focus on how the profiles changes in the sawtooth crash process itself and not on the crash conditions.

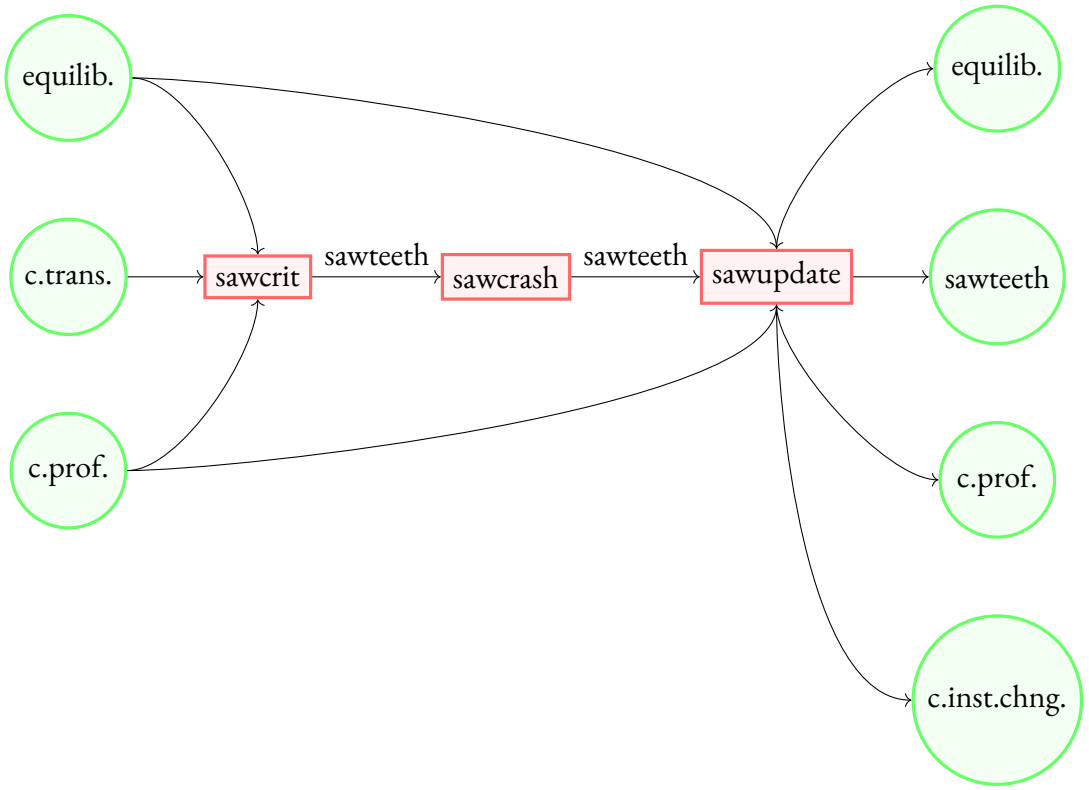

Figure 3.1: Flowchart of the sawteeth sub-workflow. The red rectangles represent the three actors: sawcrit, sawcrash, and sawupdate. The green circles represent the input and output IDSs of the sub-workflow, i.e. the inputs: equilibrium, core transport, and core profiles and the outputs: equilibrium, sawteeth, core profiles, and core instant changes. The only IDS that is passed internally between the actors is the sawteeth IDS.

4

Results

In this chapter, the resulting safety factor q, helical flux Ψ_*, electron density n_e, electron temperature T_e, and toroidal current density j_ϕ profiles in the event of a sawtooth crash in JET shot 99971 according to the Kadomtsev and Porcelli models are analysed. These results are arrived at from running the code described in section 3.2 via the workflow shown in figure 3.1. Setting the free parameter c_w to 0.8 and 1.0 for the critical island width in the Porcelli model yields two separate results for each profile and they are compared with each other, as well as with the results from the Kadomtsev model and the pre-crash profiles.

4.1 Helical flux Ψ_* profiles

The resulting Ψ_* profiles for an event of a sawtooth crash in JET shot 99971 according to the Kadomtsev and Porcelli (with $c_w = 0.8$ and 1.0) models, as well as the pre-crash profile, are shown in figure 4.1, both in full in figure 4.1a and zoomed in near the core of the plasma in figure 4.1b. Note that, Ψ_* remains more or less unchanged outside of the mixing radius r_{mix} which corresponds with the normalised generalised toroidal flux coordinate

$$\hat{\rho}_\Phi = \left(\hat{\rho}_\Phi\right)_{\text{mix}} \gtrsim 0.4$$

and that there is a corner in Ψ_* at the mixing radius for all three of the post-crash profiles. Also note that, in the Porcelli model, Ψ_* is constant for all

$$\hat{\rho}_\Phi < \left(\hat{\rho}_\Phi\right)_{\text{mix}} \quad \text{for } c_w = 1.0$$

and also constant at the same value for

$$0.1 \approx \left(\left(\hat{\rho}_\Phi\right)_{\text{crit}}\right)_- \lesssim \hat{\rho}_\Phi \lesssim \left(\hat{\rho}_\Phi\right)_{\text{mix}} \quad \text{for } c_w = 0.8,$$

while Ψ_* is parabolic for

$$\hat{\rho}_\Phi < \left(\left(\hat{\rho}_\Phi\right)_{\text{crit}}\right)_- \quad \text{for } c_w = 0.8.$$

In the Kadomtsev model, at $\hat{\rho}_\Phi = 0$, Ψ_* equals the minimum value of the pre-crash Ψ_* which occurs at the pre-crash $q = 1$ surface at $\left(\hat{\rho}_\Phi\right)_1 \approx 0.3$. Then, the post-crash profile gradually increases outwards until the mixing radius where it reaches the pre-crash value.

4.2 Safety factor q profiles

The resulting q profiles for an event of a sawtooth crash in JET shot 99971 according to the Kadomtsev and Porcelli (with $c_w = 0.8$ and 1.0) models, as well as the pre-crash profile, are

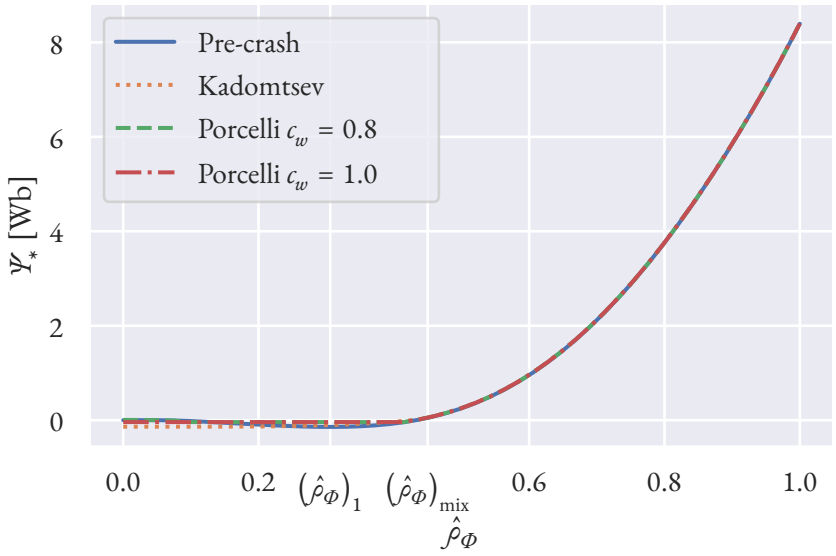

(a) Full Ψ_* profiles.

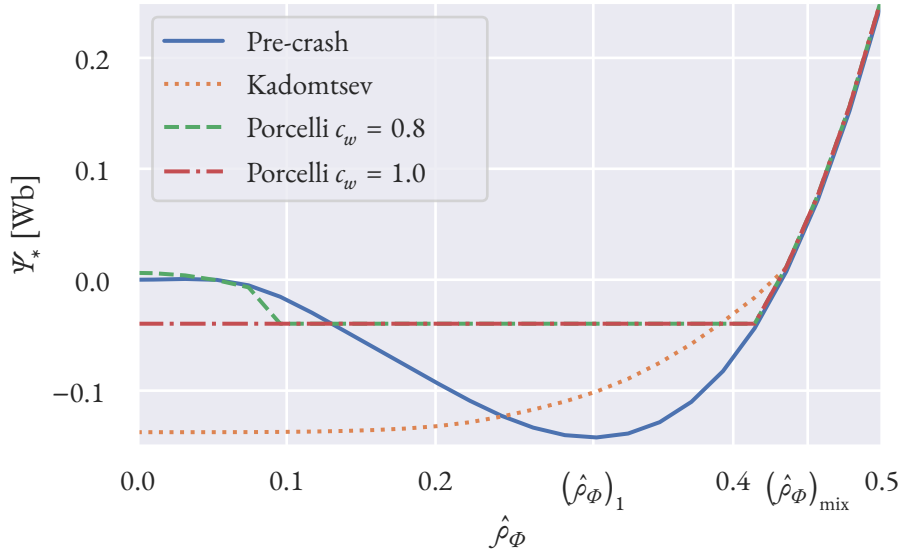

(b) Zoomed in Ψ_* profiles.

Figure 4.1: Pre-crash and crash helical flux Ψ_* profiles, for an event of a sawtooth crash in JET shot 99971 according to the Kadomtsev and Porcelli (with $c_w = 0.8$ and 1.0) models. Shown with respect to the normalised generalised toroidal flux coordinate $\hat{\rho}_\Phi$.

shown in figure 4.2, both in full in figure 4.2a and zoomed in near the core of the plasma in figure 4.2b. Note that, q remains more or less unchanged outside of the mixing radius r_{mix} which corresponds with the normalised generalised toroidal flux coordinate

$$\hat{\rho}_\Phi = \left(\hat{\rho}_\Phi\right)_{\text{mix}} \gtrsim 0.4$$

and the significant jump in q at the mixing radius for all three of the post-crash profiles. Also note that, in the Kadomtsev model, $q = 1$ at $\hat{\rho}_\Phi = 0$, which then slightly gradually increases towards $(\hat{\rho}_\Phi)_{\text{mix}}$, while, in the Porcelli model, $q = 1$ for all

$$\hat{\rho}_\Phi \lesssim \left(\hat{\rho}_\Phi\right)_{\text{mix}} \quad \text{for } c_w = 1.0$$

and $q \approx 1$ for

$$0.1 \approx \left(\left(\hat{\rho}_\Phi\right)_{\text{crit}}\right)_- \lesssim \hat{\rho}_\Phi \lesssim \left(\hat{\rho}_\Phi\right)_{\text{mix}} \quad \text{for } c_w = 0.8.$$

However, for $\hat{\rho}_\Phi < ((\hat{\rho}_\Phi)_{\text{crit}})_-$ the resulting q from $c_w = 0.8$ is not particularly flat, in contrast with what it should be according to the theoretical model.

4.3 Electron density n_e profiles

The resulting n_e profiles for an event of a sawtooth crash in JET shot 99971 according to the Kadomtsev and Porcelli (with $c_w = 0.8$ and 1.0) models, as well as the pre-crash profile, are shown in figure 4.3. Importantly, comparing the post-crash profiles to the pre-crash profile show an outwards transport of matter in the plasma, characteristic for a sawtooth crash. Note that n_e remains more or less unchanged outside of the mixing radius r_{mix} which corresponds with the normalised generalised toroidal flux coordinate

$$\hat{\rho}_\Phi = \left(\hat{\rho}_\Phi\right)_{\text{mix}} \gtrsim 0.4$$

and the significant jump in n_e at the mixing radius for all three of the post-crash profiles. Also note that, in the Porcelli model, n_e is constant for all

$$\hat{\rho}_\Phi < \left(\hat{\rho}_\Phi\right)_{\text{mix}} \quad \text{for } c_w = 1.0$$

and also constant at a slightly lower value for

$$0.1 \approx \left(\left(\hat{\rho}_\Phi\right)_{\text{crit}}\right)_- \lesssim \hat{\rho}_\Phi \lesssim \left(\hat{\rho}_\Phi\right)_{\text{mix}} \quad \text{for } c_w = 0.8,$$

while n_e is constant at a significantly higher value for

$$\hat{\rho}_\Phi < \left(\left(\hat{\rho}_\Phi\right)_{\text{crit}}\right)_- \quad \text{for } c_w = 0.8.$$

In the Kadomtsev model, n_e gradually increases from being significantly lower than what it was pre-crash for

$$0 \leq \hat{\rho}_\Phi \lesssim \left(\hat{\rho}_\Phi\right)_1 \approx 0.3,$$

to being equal at $\hat{\rho}_\Phi \approx (\hat{\rho}_\Phi)_1$, and has larger values for

$$\left(\hat{\rho}_\Phi\right)_1 \lesssim \hat{\rho}_\Phi < \left(\hat{\rho}_\Phi\right)_{\text{mix}}.$$

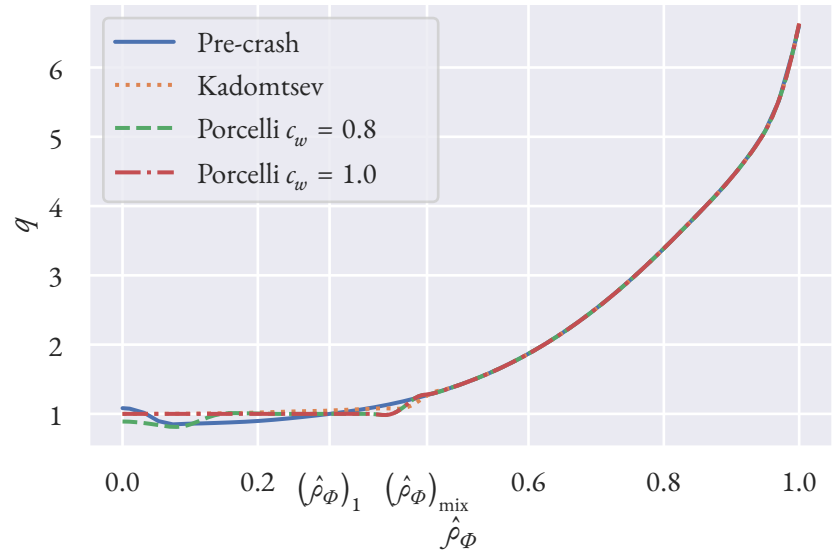

(a) Full q profiles.

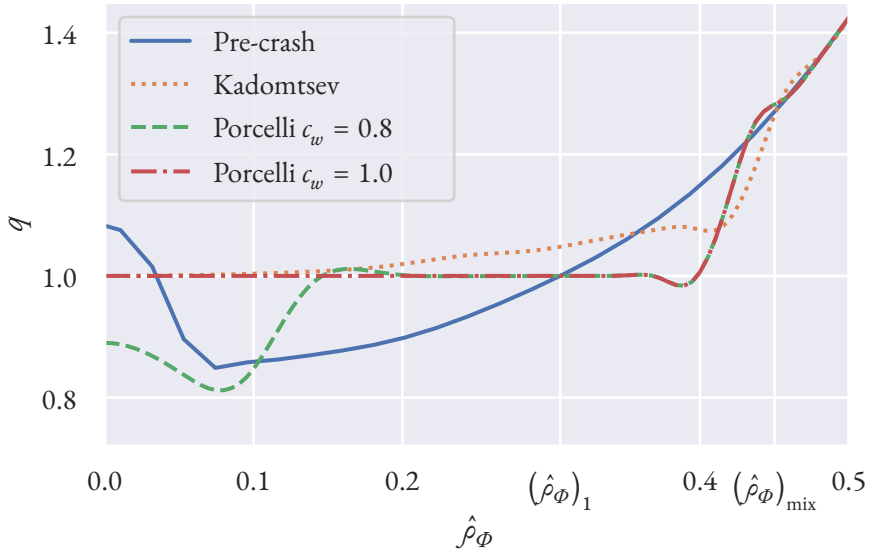

(b) Zoomed in q profiles.

Figure 4.2: Pre-crash and crash safety factor q profiles, for an event of a sawtooth crash in JET shot 99971 according to the Kadomtsev and Porcelli (with c_w = 0.8 and 1.0) models. Shown with respect to the normalised generalised toroidal flux coordinate $\hat{\rho}_\Phi$.

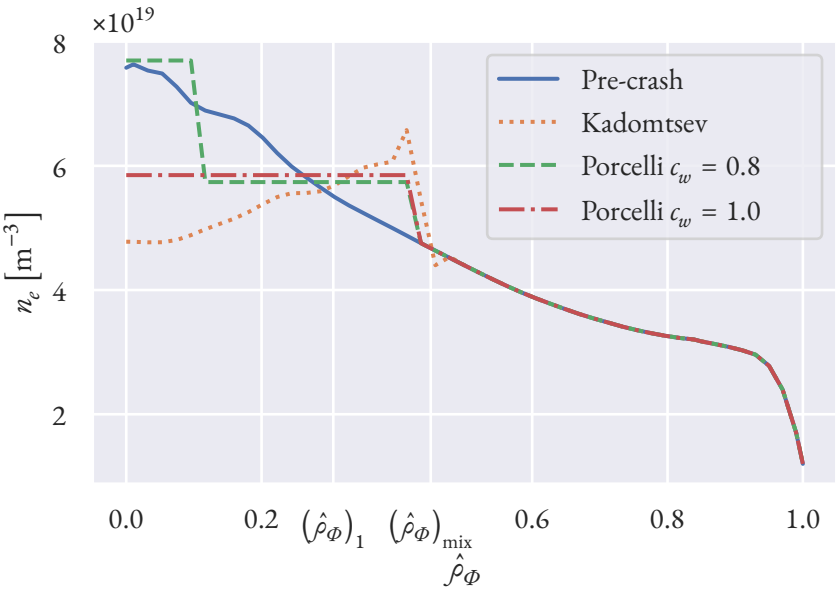

Figure 4.3: Pre-crash and crash electron density n_e profiles, for an event of a sawtooth crash in JET shot 99971 according to the Kadomtsev and Porcelli (with $c_w = 0.8$ and 1.0) models. Shown with respect to the normalised generalised toroidal flux coordinate $\hat{\rho}_\Phi$.

4.4 Electron temperature T_e profiles

The resulting T_e profiles for an event of a sawtooth crash in JET shot 99971 according to the Kadomtsev and Porcelli (with $c_w = 0.8$ and 1.0) models, as well as the pre-crash profile, are shown in figure 4.4. Importantly, comparing the post-crash profiles to the pre-crash profile show an outwards transport of temperature, i.e. kinetic energy, in the plasma, characteristic for a sawtooth crash. Note that T_e remains more or less unchanged outside of the mixing radius r_{mix} which corresponds with the normalised generalised toroidal flux coordinate

$$\hat{\rho}_\Phi = \left(\hat{\rho}_\Phi\right)_{\text{mix}} \gtrsim 0.4$$

and the significant jump in T_e at the mixing radius for all three of the post-crash profiles. Also note that, in the Porcelli model, T_e is constant for all

$$\hat{\rho}_\Phi < \left(\hat{\rho}_\Phi\right)_{\text{mix}} \quad \text{for } c_w = 1.0$$

and also constant at a slightly lower value for

$$0.1 \approx \left(\left(\hat{\rho}_\Phi\right)_{\text{crit}}\right)_- \lesssim \hat{\rho}_\Phi \lesssim \left(\hat{\rho}_\Phi\right)_{\text{mix}} \quad \text{for } c_w = 0.8,$$

while T_e is constant at a significantly higher value for

$$\hat{\rho}_\Phi < \left(\left(\hat{\rho}_\Phi\right)_{\text{crit}}\right)_- \quad \text{for } c_w = 0.8.$$

In the Kadomtsev model, T_e gradually increases from being significantly lower than what it was pre-crash for

$$0 \leq \hat{\rho}_\Phi \lesssim \left(\hat{\rho}_\Phi\right)_1 \approx 0.3,$$

to being equal at $\hat{\rho}_\Phi \approx (\hat{\rho}_\Phi)_1$, and has larger values for

$$(\hat{\rho}_\Phi)_1 \lesssim \hat{\rho}_\Phi < (\hat{\rho}_\Phi)_{\text{mix}}.$$

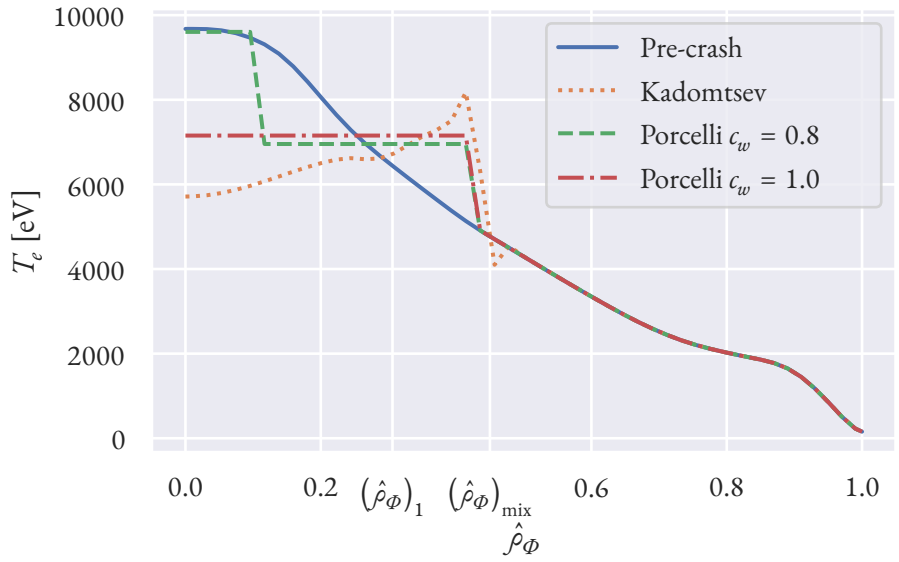

Figure 4.4: Pre-crash and crash electron temperature T_e profiles, for an event of a sawtooth crash in JET shot 99971 according to the Kadomtsev and Porcelli (with $c_w = 0.8$ and 1.0) models. Shown with respect to the normalised generalised toroidal flux coordinate $\hat{\rho}_\Phi$.

4.5 Toroidal current density j_ϕ profiles

The resulting j_ϕ profiles for an event of a sawtooth crash in JET shot 99971 according to the Kadomtsev and Porcelli (with $c_w = 0.8$ and 1.0) models, as well as the pre-crash profile, are shown in figure 4.5. Note the major spike at the mixing radius r_{mix} which corresponds with the normalised generalised toroidal flux coordinate

$$\hat{\rho}_\Phi = (\hat{\rho}_\Phi)_{\text{mix}} \gtrsim 0.4$$

and the smaller spikes at $\hat{\rho}_\Phi = 0$ and $\hat{\rho}_\Phi = 1$ in all the crash j_ϕ profiles, as well as the moderately large spike at

$$\hat{\rho}_\Phi \approx \left((\hat{\rho}_\Phi)_{\text{crit}}\right)_- \approx 0.1 \quad \text{for } c_w = 0.8,$$

all representing the unphysical current sheets that are inherently present in both models.

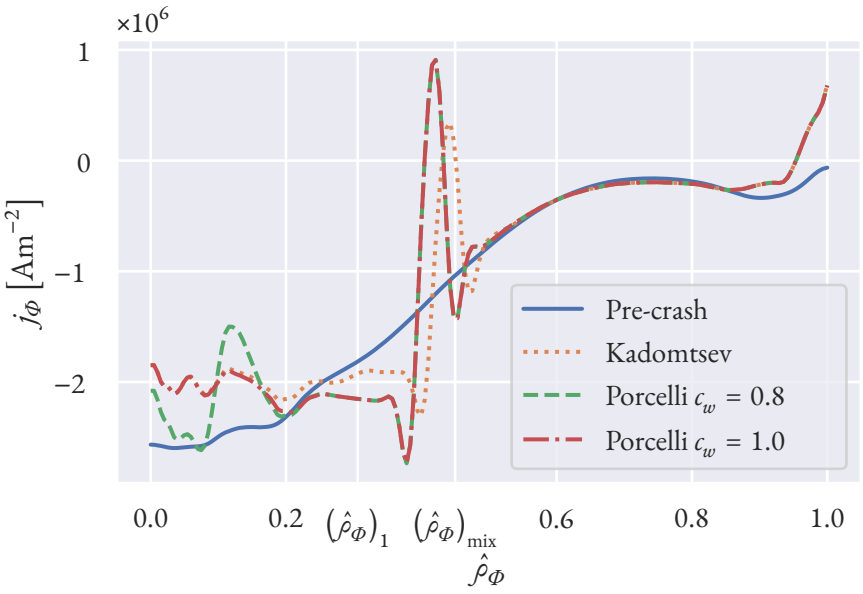

Figure 4.5: Pre-crash and crash toroidal current density j_ϕ profiles, for an event of a sawtooth crash in JET shot 99971 according to the Kadomtsev and Porcelli (with $c_w = 0.8$ and 1.0) models. Shown with respect to the normalised generalised toroidal flux coordinate $\hat{\rho}_\Phi$.

5

Discussion

Over all, the simulation results presented in the previous chapter are quite good in terms of the implementation of the theoretical models being correct. In particular, the Ψ_* post-crash profiles clearly shows the characteristics that we expect from the Kadomtsev and Porcelli models and the q profiles are also mostly good in this regard. The outwash of density and temperature that leads to the sudden drop in power output in a sawtooth crash is also clearly seen in the n_e and T_e post-crash profiles, which are both well behaved according to the models too. While the discontinuities and non-smoothness in all of these profiles and the resulting current sheets that are represented as spikes in the j_ϕ profiles are unphysical, these are inherent to the models themselves and not a sign of them being incorrectly implemented.

However, one inaccuracy can be identified in the

$$0 \leq \hat{\rho}_\Phi < \left(\left(\hat{\rho}_\Phi\right)_{\text{crit}}\right)_-$$

region, where the crash q profile from the Porcelli model with $c_w = 0.8$, see figure 4.2, is not as constant as one might expect after considering the theoretical model. This numerical artifact is a result of q being calculated from the derivative of an interpolated Ψ_* profile. There are also smaller artifacts for all of the post-crash profiles around $\left(\hat{\rho}_\Phi\right)_{\text{mix}}$ for the same reason. These artifacts are most likely a result of the resolution of the input profiles not being high enough for numerical accuracy, but it could of course also mean that the implementation is not entirely accurate compared with the theoretical models. However, this is not a great cause for concern, since a discontinuous q profile is non-physical and leads to issues if used as input to the equilibrium calculating actors in ETS, meaning that output from completely accurate implementations of the Kadomtsev and Porcelli models might need to be smoothed for certain calculations to be possible anyway. That said, the unintentional smoothing effect from the artifacts we see in figure 4.2b is most likely not enough compared to how inaccurate the results become, so some other, more rigorous, smoothing method, such as a smoothing interpolation, that avoids the inaccuracies is probably a better option.

The unphysical current sheets we see as spikes in the crash current density profiles will certainly cause issues for equilibrium propagation calculations, since the very large current gradients will result in large pressure gradients that will drive instabilities and make the calculated equilibrium way more unstable than what it should be from a physical standpoint. This issue could potentially be avoided if a more advanced model were to be used instead of the Kadomtsev and Porcelli models, since the crash current profile could be flatter in that case, which it is per design in the FCM (Fischer et al. 2019), making it a reasonable candidate for use in future work in sawteeth simulations.

5.1 Workflow implementation

The inputs and outputs of the sawteeth sub-workflow not being balanced, i.e. the same IDS types, could also cause issues. When an actor outputs data to an IDS type that it did not receive as input, it needs to generate a new IDS of that type. For instance, the sawupdate actor puts some of its output in the core instant changes IDS, which is not a previously initiated IDS in the sawteeth sub-workflow visualised in figure 3.1. Thus, the affected IDSs will only contain data for single time steps, so the data will not be properly accessible for other actors, which could lead to them having less accurate output, generally preforming worse, or even halting, if they need to analyse some time dependency. Additionally, it is more efficient to allocate the necessary computer resources to save the data in the IDSs all at once, so to do some of it at every time step is of course simply wasteful.

6

Conclusion

This thesis has studied the physics of the sawtooth instability in tokamak plasmas and converted an existing implementation of the Kadomtsev and Porcelli models from using CPOs to IDSs. This implementation was then used to simulate the post-crash profiles in a IMAS-PAF workflow and when comparing the results to what should be expected of the theoretical models, it is clear that the CPO to IDS conversion was successful.

The process of upgrading the sawteeth actors and working with them in general, has resulted in a gained understanding of the physics involved, in particular according to the Kadomtsev and Porcelli models, in sawteeth oscillations in tokamak plasmas and the technical aspects of the simulation frameworks are structured. Hopefully, this understanding has been reflected throughout the entirety of this thesis, and in particular in the explanations in chapter 2 of how the sawtooth phenomenon manifests in tokamak reactors, as well as in the descriptions in chapter 3 of all said technical aspects.

Unfortunately, it proved too difficult and, above all, too time consuming to extend the scope of the thesis to include the sawteeth actors in a time loop simulation workflow, but some of the issues that need to be resolved to achieve this have been identified and discussed. The most significant being the unphysical current sheets and the non-smoothness in the post-crash profiles, since the actors that preform the equilibrium calculations, using j_ϕ as input, will not work properly as a result. This insight, in combination with the data structure conversion and the knowledge gained about the subject and field, is still a significant step towards a working sawtooth model being available for use in ETS-PAF or other simulators running on the same framework.

6.1 Next steps

While this thesis has reached its end and conclusion, the work towards a fully functional sawtooth model, being implemented in ETS-PAF will not end. Some immediate steps will be taken towards including the sawteeth sub-workflow in a time loop workflow. As previously discussed, this might be more or less problematic, primarily since the post-crash profiles are probably not well enough behaved for the time propagation calculating actors to handle. Depending on how severe this issue turns out to be, it might be sufficient to apply some simple smoothing on the current output, i.e. turn the model into an ad hoc approximation of the Kadomtsev or Porcelli model. On the other hand, if the problem is bad enough, it could be necessary to look into implementing some other, more advanced, model, one candidate being a FCM (Fischer et al. 2019), which might be interesting to eventually implement anyway.

Another idea for continued development, that is probably less difficult to implement, is turning on the complete set of crash conditions and tune the crash parameters to give an expected sawtooth period for some relevant test case that could be decided on in collaboration with ITER. This test case should be similar enough to expected operation conditions, such that the same tuning of the parameters could be used for predictive runs, when determining how to control and minimise the negative effects of the sawtooth and other instabilities. However, the sawtooth period can of course only be predicted properly after having a simulation run through multiple sawtooth crashes, meaning that this development is only possible after the sawteeth model is running well in a working time loop, making that an obvious priority.

A third way to increase the usefulness of the current sawteeth model implementation, would be to look further into how the sudden sawtooth crash events interact with other plasma instabilities and see if it is possible to model these interactions in the workflows. Since a parallel thesis project on the NTM instability, carried out by another master student, also will continue in a similar way to this one, focus will be put, by collaborative effort, on how the sawtooth crashes may trigger NTM through so called seed islands.

How long all of these intended future developments will take and how difficult they are going to be to complete, is difficult to predict and some of it all might need to be left for others working in the field. This would clearly be a daunting task for anyone previously not fully involved in the details of the project, but it will be a much less complicated task than what it otherwise would be if a sawteeth model can be successfully included in a time loop and the characteristic sawteeth waves can be produced for some relevant test case. If at least that is achieved, this thesis project and its continuation should certainly be considered a success.

Bibliography

Anderson, Dan, Mietek Lisak, Pontus Johannisson and Mattias Marklund (2003). *Basic Plasma Physics. Theory and Applications*. Provided as course material for Plasma Physics with Applications RRY085, at Chalmers University of Technology.

Antonsen T. M., Jr., J. F. Drake, P. N. Guzdar, A. B. Hassam, Y. T. Lau, C. S. Liu and S. V. Novakovskii (June 1996). "Physical mechanism of enhanced stability from negative shear in tokamaks: Implications for edge transport and the L-H transition". In: *Physics of Plasmas* 3.6, pp. 2221–2223. ISSN: 1070-664X. DOI: 10.1063/1.871928.

Bellan, Paul M. (2006). *Fundamentals of Plasma Physics*. Cambridge University Press.

Chapman, Ian T. (2015). "Sawtooth Instability". In: *Active Control of Magneto-hydrodynamic Instabilities in Hot Plasmas*. Ed. by Valentin Igochine. Springer Series on Atomic, Optical, and Plasma Physics (SSAOPP), vol. 83. Springer Berlin Heidelberg. Chap. 4, pp. 105–142. ISBN: 978-3-662-44222-7. DOI: 10.1007/978-3-662-44222-7_4.

Coster, David (9th Dec. 2024). *Using the IMAS Persistent Actor Framework for implementing the European Transport Simulator*. [Conference presentation]. Max-Planck-Institut für Plasmaphysik.

Fischer, R., A. Bock, A. Burckhart, O. P. Ford, L. Giannone, V. Igochine, M. Weiland, M. Willensdorfer and the ASDEX Upgrade Team (Mar. 2019). "Sawtooth induced q-profile evolution at ASDEX Upgrade". In: *Nucl. Fusion* 59.5, p. 056010. ISSN: 1741-4326. DOI: 10.1088/1741-4326/ab0b65.

Freidberg, Jeffrey P. (2007). *Plasma Physics and Fusion Energy*. Cambridge University Press. ISBN: 978-0-521-85107-7. DOI: 10.1017/CBO9780511755705.

Igochine, Valentin (Dec. 2023). "Magnetic reconnection during sawteeth crashes". In: *Physics of Plasmas* 30.12, p. 120502. ISSN: 1070-664X. DOI: 10.1063/5.0169243.

JET's salient features (2014). EUROfusion Consortium Research Institutions. URL: https://euro-fusion.org/devices/jet/jets-salient-features/ (visited on 01/10/2025).

Kadomtsev, B. B. (1975). "Disruptive instability in Tokamaks". In: *Fizika Plazmy* 1, pp. 710–715. English translation in: *Soviet Journal of Plasma Physics* 1, pp. 389–391.

Merle, A. (14th Oct. 2015). *European Transport Solver - Physics Capabilities. Sawteeth Model*. [Conference presentation]. EUROfusion Science Meeting. Ecole Polytechnique Fédérale de Lausanne (EPFL), Swiss Plasma Center (SPC), CH-1015 Lausanne, Switzerland.

– (10th Mar. 2016). *European Transport Solver. Sawteeth Model*. [Conference presentation]. ETS4JET training. Ecole Polytechnique Fédérale de Lausanne (EPFL), Swiss Plasma Center (SPC), CH-1015 Lausanne, Switzerland.

Porcelli, F, D. Boucher and M. N. Rosenbluth (Dec. 1996). "Model for the sawtooth period and amplitude". In: *Plasma Physics and Controlled Fusion* 38.12, p. 2163. DOI: 10.1088/0741-3335/38/12/010.

Sauter, O. and S. Yu. Medvedev (2013). "Tokamak coordinate conventions: COCOS". In: *Computer Physics Communications* 184.2, pp. 293–302. ISSN: 0010-4655. DOI: 10.1016/j.cpc.2012.09.010.

Veen, Lourens E. and Alfons G. Hoekstra (2020). "Easing Multiscale Model Design and Coupling with MUSCLE 3". In: *Computational Science – ICCS 2020*. Ed. by Valeria V. Krzhizhanovskaya, Gábor Závodszky, Michael H. Lees, Jack J. Dongarra, Peter M. A. Sloot, Sérgio Brissos and João Teixeira. Lecture Notes in Computer Science (LNTCS), vol. 12142. Cham: Springer International Publishing, pp. 425–438. ISBN: 978-3-030-50433-5. DOI: 10.1007/978-3-030-50433-5_33.

Wesson, John (2004). *Tokamaks*. 3rd ed. International Series of Monographs on Physics 118. Oxford, England: Clarendon Press. ISBN: 0-198-50922-7.

DEPARTMENT OF SPACE, EARTH AND ENVIRONMENT
CHALMERS UNIVERSITY OF TECHNOLOGY
Gothenburg, Sweden
www.chalmers.se

CHALMERS
UNIVERSITY OF TECHNOLOGY